

Depth Estimation and Image Restoration by Deep Learning from Defocused Images

Saqib Nazir, *Student Member, IEEE*, Lorenzo Vaquero, Manuel Mucientes, Víctor M. Brea, and Daniela Coltuc

Abstract—Monocular depth estimation and image deblurring are two fundamental tasks in computer vision, given their crucial role in understanding 3D scenes. Performing any of them by relying on a single image is an ill-posed problem. The recent advances in the field of deep convolutional neural networks (DNNs) have revolutionized many tasks in computer vision, including depth estimation and image deblurring. When it comes to use defocused images, the depth estimation and the recovery of the All-in-Focus (AiF) image become related problems due to defocus physics. In spite of this, most of existing models treat them separately. There are, however, recent models that solve these problems simultaneously by concatenating two networks in a sequence to first estimate the depth or defocus map and then reconstruct the focused image based on it. We propose a DNN that solves the depth estimation and image deblurring in parallel. Our Two-headed Depth Estimation and Deblurring Network (2HDED:NET) extends a conventional Depth from Defocus (DFD) networks with a deblurring branch that shares the same encoder as the depth branch. The proposed method has been successfully tested on two benchmarks, one for indoor and the other for outdoor scenes: NYU-v2 and Make3D. Extensive experiments with 2HDED:NET on these benchmarks have demonstrated superior or close performances to those of the state-of-the-art models for depth estimation and image deblurring.

Index Terms—Depth from Defocus, Image Deblurring, Deep learning

I. INTRODUCTION

DEPTH estimation from a single image is a key problem in computer vision, where it spans a lot of applications. Robotics, augmented reality, human computer interaction or computational photography, to give only several examples, benefit from the depth estimation. With the recent advancements in 3D computer vision and the newly emerging tasks

This project has received funding from the European Union's Horizon 2020 research and innovation programme under the Marie Skłodowska-Curie grant agreement No. 860370. The last author acknowledges financial support from UEFISCDI Romania grant 31/01.01.2021 PN III, 3.6 Suport. This research was also partially funded by the Spanish Ministerio de Ciencia e Innovación [grant number PID2020-112623GB-I00], and the Galician Consellería de Cultura, Educación e Universidade [grant numbers ED431C 2018/29, ED431C 2021/048, ED431G 2019/04]. These grants are co-funded by the European Regional Development Fund (ERDF). Lorenzo Vaquero is supported by the Spanish Ministerio de Universidades under the FPU national plan (FPU18/03174).

S. Nazir and D. Coltuc are with CEOSpaceTech, University POLITEHNICA of Bucharest (UPB), Bucharest, Romania (e-mail: saqib.nazir@upb.ro ; daniela.coltuc@upb.ro).

L. Vaquero, M. Mucientes and V. Brea are with Centro Singular de Investigación en Tecnoloxías Intelixentes (CITIUS) University of Santiago de Compostela (USC), Santiago de Compostela, Spain (e-mail: lorenzo.vaquero.otal@usc.es; manuel.mucientes@usc.es ; victor.brea@usc.es).

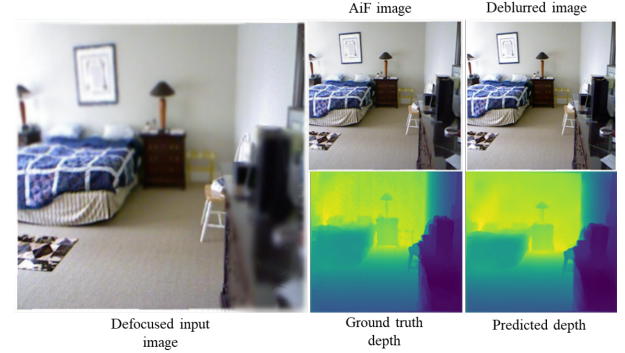


Fig. 1. Example of image deblurring and depth prediction using 2HDED:NET in a scene from the NYU-v2 dataset. AiF is an all-in-focus image that serves as ground truth for deblurring. The AiF and ground-truth depth are captured by an RGBD Kinect camera.

like semantic segmentation or 3D object detection, depth estimation has become even more important.

The depth can be measured by specialized devices or can be inferred from images and videos. For outdoor scenes, LIDAR or stereo systems are typically used to measure the depth of scene. For indoor scenes, Time of Flight (ToF) cameras like RGBD Kinect from Microsoft, are used to capture depth information in addition to RGB images. Such devices have their limitations. ToF cameras are not working properly in the outdoors, being limited to 30m at best, while the LIDAR may produce poor quality depth maps because of the infrared interference. These physical limitations, the sparse nature of the measurements, and sometimes the cost of the devices has fostered the research in the direction of obtaining depth from images or videos taken with commercial cameras. Here, although the performance of depth estimation methods is steadily increasing, there are still major problems related to the accuracy and resolution of the estimated depth maps.

Image deblurring is a classical problem in low level computer vision, and a preprocessing step in numerous applications such as face detection, classification, object recognition or misfocus correction. Object motion, camera shake, or out-of-focus are common causes for the blur appearing in the images taken with a camera. The goal of image deblurring is to recover an AiF image with all the details and sharp edges from its defocused counterpart.

The goal of the network proposed in this paper is to estimate depth and remove blur from a single out-of-focus image. Fig. 1 shows an example of Depth from Defocus (DFD) and

image deblurring. Here, the goal has been to estimate a dense depth map and meanwhile, reconstruct the AiF image from a defocused input image.

Most of DNNs dedicated to depth estimation work on AiF images [1]–[3]. The exploitable information in such images is limited to the scene geometry, which explains the lower performances compared to LIDAR or ToF camera. The defocus blur is a complementary cue that can help to improve the depth accuracy.

DFD has been widely investigated in the past [4]. The first DFD methods were focused on the depth related to the blur amount and for this reason, they suffered from insensitivity in the Depth of Field (DoF) region and uncertainty regarding the object position with respect to the in-focus plane. The use of coded apertures [5], [6], dual images or focal stacks [7]–[9] has alleviated such problems.

In many applications, DNN models outperform the classical methods due to the ability of learning more complex features. It is also the case of DNN models dedicated to DFD [10]–[13]. The features they learn from defocused images combine both the scene geometry and the blur to estimate more accurately the depth. In the last years, a series of DNNs has been proposed for image deblurring as well [10], [14]–[17].

Although the depth and defocus blur are closely related, the deblurring and depth estimation have been generally treated as separate problems by deep learning. There are however some rare exceptions like the method of Anwar et al. [10], which concatenates two networks to first estimate the depth map and then, based on this depth, restores a focused image by pixel wise non-blind deconvolution. More precisely, in [10] a fully convolutional neural network with 13 layers provides a pixel level feature map, then a patch pooling layer turns the patches around predefined key points into fixed size feature map, which are further propagated through a shallow fully connected network to estimate a dense depth map. The deblurring is done by deconvolution with kernels calculated for every pixel of the RGB image, by using the estimated depth.

Architectures with independent and task-dedicated branches and their loss terms combined decrease overfitting in the training phase, and permit to execute any of the tasks in the inference time. In this line, we propose a DNN that solves the problem of DFD and image deblurring in parallel. It is a two headed network called 2HDED:NET, that estimates the depth and deblurs the image in a balanced way by giving the same importance to both tasks. The network consists of three modules: i) an encoder for multi-level feature extraction from the out-of-focus image, ii) a depth estimation decoder (DED) for the task of DFD, iii) an AiF decoder (AifD) for image deblurring (Fig. 2). The heads interact with each other during training, allowing the encoder to learn semantically rich features that are well suited for both tasks.

Unlike Anwar et al. in [10], where the deblurring depends on the intermediate result of depth estimation, our 2HDED:NET generates an AiF image, which is not anymore constrained by depth accuracy. Separating the deblurring and depth estimation branches also makes AifD self-sufficient and better able to perform the deblurring task without relying on

an estimated depth map.

2HDED:NET is a typical Multitask Learning (MTL) neural network with hard sharing of parameters. The encoder layers are shared by both depth estimation and deblurring tasks while the two decoders remain task-specific. Comparing to single task networks, the MTL networks benefit from a series of advantages: an augmented training set, relevant feature learning by attention focusing, easier learning of features from less complex models, reduced risk of overfitting and better generalization to new tasks [21]. The foundations of MTL by hard parameter sharing had been laid by Caruana in 1997 [18], two recent surveys of MTL can be found in [19], [20]. The MTL technique has been used successfully in computer vision application as well as in other areas like natural language processing or drug discovery. Two recent applications closely related to our application are addressed in [21], [22], where the depth map and a semantic segmentation are learned by MTL.

The architecture of 2HDED:NET is straightforward, simple, and easy to train. With its double functionality – depth estimation and deblurring – 2HDED:NET emulates a Kinect type camera on a commercial camera with limited DoF. A special feature of 2HDED:NET is that after training, the depth estimation head is no longer necessary to recover a sharp image and vice versa.

We define a hybrid loss function to train 2HDED:NET. It embeds specific losses for depth and deblurring like $L1$ norm and Charbonier loss [11], [23] as well as specific regularization like gradient based smoothing [24] and maximization of Structural Similarity Index Measure (SSIM).

We run extensive experiments on the NYU-v2 and Maked3D benchmarks in order to evaluate the performances of the 2HDED:NET and to compare them with state-of-the-art methods for depth estimation and image deblurring. In most of the cases, 2HDED:NET generates better results. For training, 2HDED:NET uses two types of ground truth, the depth and the AiF images in the benchmarks. As input, we generate synthetically defocused images by using the thin lens model. Thus, the a priori information is like for any other network for depth estimation. The supplement is the mathematical model of the defocus blur that proves through our results its effectiveness.

The main scientific contributions of our work are:

- A novel architecture, 2HDED:NET, that recovers the AiF images and generates the depth map from a single defocused image.
- The architecture is the first of its kind to generate the depth map and AiF images in a balanced way and attaching the same importance to both tasks.
- A hybrid loss function that combines losses and regularizations from both depth estimation and deblurring and enforces the encoder to learn much richer semantic features.
- Experimental results on NYU-v2 and Make3D datasets enriched with synthetic defocused images, which confirm the effectiveness of our approach.

The remainder of this paper is organized as follows. In Section II, we provide an overview of the related work. In

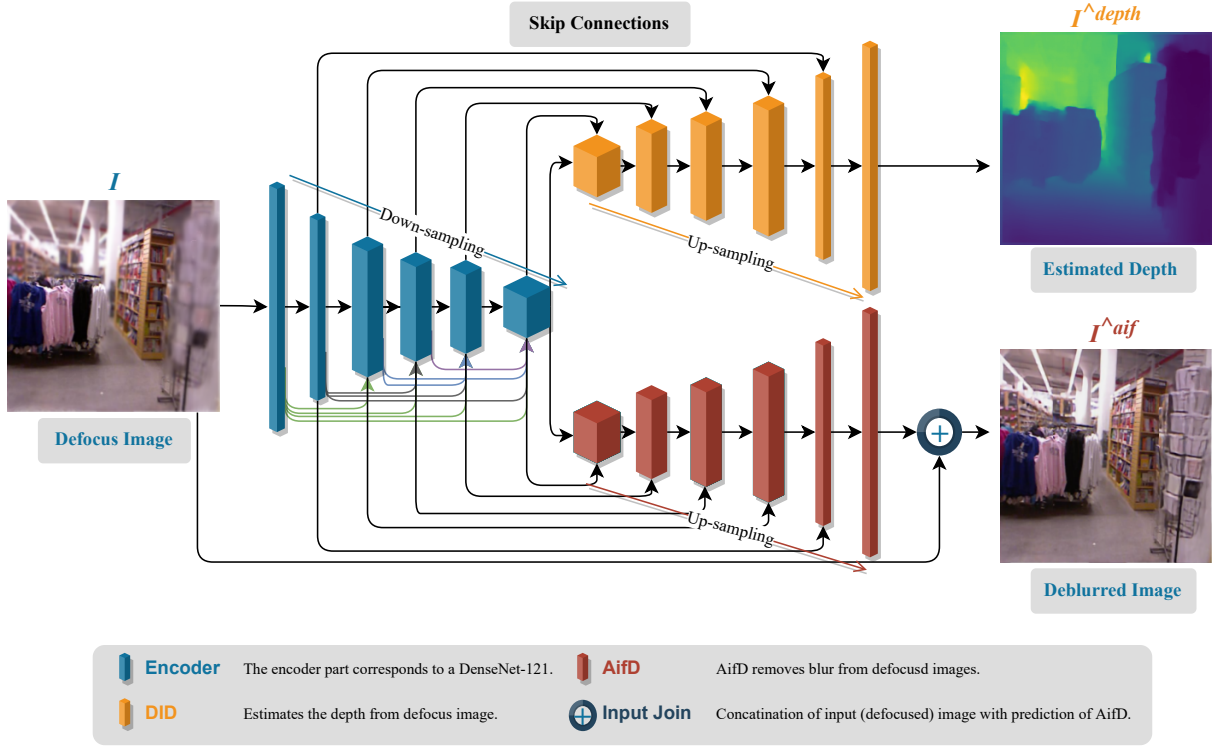


Fig. 2. 2HDED:NET architecture from [25], consists of one encoder and two decoders that work in parallel. The upper Head estimates the depth map and the lower one the AiF image. The network is fed in with defocused RGB images.

Section III, we present our methodology. The experimental setup and results are reported in Sections IV, and V, and, finally, in Section VI, we present conclusions and future work.

II. RELATED WORK

This section briefly reviews several DNNs based solutions for DFD and deblurring, which make up the current state of the art.

A. Single image depth estimation

The success of DNN models in various fields of computer vision, such as image segmentation and classification, has prompted the scientific community to consider using DNNs for depth estimation as well. Saxena et al. [2] presented one of the first solutions for monocular depth estimation with deep learning methods. They estimate the depth with a multi-scale architecture and the Markov Random Field (MRF). Eigen et al. [3] presented one of the most successful work by developing a multi-scale architecture to extract information from a scene at global and local levels in order to estimate the depth map. Laina et al. [26] proposed an encoder-decoder network with a fast up-projection block. Cao et al. [27] rely on Conditional Random Fields (CRF) to improve the accuracy of depth maps. GANs have also been utilized for depth prediction. Jung et al. in [28] and Carvalho et al. in [29] implemented an adversarial loss for depth prediction. Most of the evoked networks solve the problem of monocular depth estimation by using in-focus images as input and ignoring the defocus blur, which is however an important cue in depth estimation.

B. Depth from defocus

Defocus blur occurs when images are captured with limited DoF. All cameras have a limited DoF, which is controlled by the camera aperture diameter. Although the blur exists also in this range, it is not perceived by the human eye.

To estimate depth from a single defocused image, Carvalho et al. [11] built on a dense network DenseNet-121 with skip connections that improved the state-of-the-art results of the time. To handle the DFD problem, Gur et al. [30] designed a convolution layer based on the point spread function (PSF) to train an unsupervised network. Anwar et al. [10] trained a fully connected cascaded deep neural network inspired by the VGG-16 model on dense overlapping fields to estimate depth from a single defocused image. In [12], Fu et al. propose a multi-scale network structure to obtain high-resolution depth maps using spacing-increasing discretization and a simple regression loss.

C. Image deblurring

Blind image deblurring has been always a difficult problem. Since the advent of DNNs, several models were designed to reduce the blur from a single image. The first ones directly remove the blur, as is the case of Nah et al. [31], who use a multiscale loss function to train their model. Tao et al. [32] improve on their work by using joint network parameters at different scales. Kupyn et al. propose DeblurGAN to reconstruct AiF images from defocused images by using an adversarial loss function [33]. Lee et al. [34] introduced a deep architecture along with a domain matching approach to

estimate the defocus map of an image, and also presented a large dataset for training DNNs.

The strategy adopted in more recent papers is to first estimate a defocus/depth map and later to use this information for image deblurring. Very recently, for estimating defocus maps, works like [10], [14] use the amount of blur per pixel to reconstruct the entire deblurred image.

Zhang Kai et al. propose in [35], [36] two general methods for image restoration, with deblurring as a particular case. In [35], it is shown that by separating the fidelity from the regularization term in the energy function, the optimization problem can be solved by plugging a denoising neural network in a Half Quadrating Splitting framework. The method is tested for denoising, super-resolution and deblurring. In [36], the authors propose a convolutional neural network for blind Gaussian denoising. The network removes the latent clean image and estimates the residual Gaussian noise with unknown level. By observing that the image degradation model for Gaussian denoising can be converted to other restoration problems, the authors successfully apply it to image super-resolution and JPEG deblocking.

The priors on image model play an important role in image restoration by optimization. Zha et al. propose in [37] a low-rank and deep image model with three complementary priors: internal and external, shallow and deep, and non-local and local priors. The model is successfully tested on image deblurring, restoration after compressive sensing and JPEG deblocking. The sole non-local self-similarity prior is used by Zha et al. in [38] for image restoration by using the Expectation Maximization algorithm with image deblurring, denoising and deblocking as applications.

D. Joint DFD and image deblurring

The survey of the literature has revealed only two DNN models that handle both depth estimation and blurring or deblurring process. Gur et al. proposed in [30] a network to estimate the depth from a single focused image. Unlike the supervised learning networks, they adopt a self-supervised learning approach with a loss function based on the difference between the defocused version of the input image and an estimate of this obtained by a second network. This second network implements the blur model and by using the estimated depth creates a synthetically defocused image.

The closest approach to our architecture is the model proposed by Anwar et al. in [10]. They train a cascade of two smaller networks to estimate a depth map, which is then used to compute kernels for restoring the AiF image by pixel-wise non-blind deconvolution.

III. 2HDED:NET ARCHITECTURE

Fig. 2 depicts the architecture of the 2HDED:NET. Given a single defocused image I , the goal of our network is to estimate the depth map \hat{I}^{depth} and to restore the AiF image \hat{I}^{aif} . As shown in Fig. 2, our 2HDED:NET mainly consists of one encoder and two decoders that output the depth map and AiF image in parallel. By utilizing the features learned by the same encoder, both heads can mutually benefit from each

other. 2HDED:NET is a supervised method i.e., it requires the ground truth depth as well as AiF images for training.

A. Encoder

For the encoder network, we use the DenseNet-121 [39]. As its name suggests, DenseNet consists of densely connected layers. The main feature of DenseNet-121 is that this network reuses the features of each layer by concatenating them with the features of the next layer, rather than simply aggregating them like ResNet50. The goal of concatenation is to use the features obtained in the previous layers in the deeper layers. This is referred to as "feature reusability". DenseNets can learn mappings with fewer parameters than a typical CNN since there are no redundant maps to learn. Similar to [11], we replace the max-pooling layer with a 4×4 convolutional layer to reduce resolution while increasing the number of feature channel maps. We use skip connections between encoder and decoder parts to simplify learning. The skip connections prevent the problem of the gradient disappearing, since the subsequent layers focus on solving residuals rather than completely new representations. The encoder helps in obtaining multi-resolution features from the input image, which are useful for the two tasks that 2HDED:NET performs. Further information about the encoder's output sizes, input and output channels can be seen in Table I.

B. Depth Estimation Head

The Depth Estimation Decoder (DED) is inspired by [11]. It consists of five decoding layers, each with a 4×4 convolution that increases the resolution of the feature map, followed by a 3×3 convolution that reduces the aliasing effect of upsampling. Batch normalization and ReLU functions are included after each convolutional layer to make learning more stable and to allow representation of nonlinearities. Table I shows how decoder layers upsample the input using transpose convolutions. The output of DED is one channel depth map.

C. Deblurring Head

We refer to the deblurring decoder as an AiF decoder (AifD). Unlike DED, the output of AifD is a three-channel RGB image. We use an input joint layer to aggregate the

TABLE I
SIZE OF OUTPUT FEATURES AND INPUT/OUTPUT CHANNELS OF EACH LAYER OF OUR ENCODER-DECODER NETWORK.

Layer	Output size	Input/C	Output/C
Conv1	128×128	3	64
Conv2	64×64	64	128
Conv3	32×32	128	256
Conv4	16×16	256	512
Conv5	8×8	512	1024
Dconv5	8×8	1024	1024
Dconv4	16×16	1024	512
Dconv3	32×32	512	256
Dconv2	64×64	256	128
Dconv1	128×128	128	64
Pred-depth	256×256	64	1
Pred-deblurring	256×256	64	3

defocused input image with the output of AifD as in [14], [40] for the final prediction. The content of the defocused image and the corresponding prediction from AifD are embedded in the input joint layer, giving to this head more detailed guidance for learning deblurring. Unlike methods that use pipeline processing, where the depth or defocus map is first predicted and then the focused image is recovered, our deblurring head is not based on such estimates, avoiding reliance on insufficient depth maps in some cases.

An important feature of our solution is that once 2HDED:NET is fully trained, we are still able to perform a task when the other head is removed, e.g. we can perform DFD without AifD head and vice versa.

D. Loss functions

The training of the 2HDED:NET is supervised simultaneously by ground truth depth maps and AiF images. To consider this dual information, we propose a loss function with two terms, one that accounts for the depth loss and another for the deblurred image. These two components are balanced as to have approximately equal contributions.

1) *Depth loss*: Most of the deep learning methods proposed for depth estimation have been trained with pixel-wise regression based loss functions calculated as mean of absolute differences (L1 norm), squared differences (L2 norm) or combinations of them [11].

As loss function for depth estimation, we resort to L1 norm, known for the ability of estimating sparse solutions as it is the case for depth maps [11]:

$$\mathcal{L}_1^{Depth} = \frac{1}{n} \sum_{i=1}^n |\hat{I}_i^{depth} - I_i^{depth}| \quad (1)$$

where \hat{I}^{depth} is the estimated depth, I^{depth} the ground truth, i is the current pixel and n is the number of pixels.

Often, this loss is complemented by a smoothing regularization term that has the role of removing the low amplitude structures in the depth map while sharpening the main edges [24], [30], [41], [42]. In the case of our network, we improve the depth accuracy by combining L1 norm with the smoothing term commonly used in supervised learning and defined as [24]:

$$\mathcal{L}_{grad} = \frac{1}{n} \sum_i |\Delta_x R_i| + |\Delta_y R_i| \quad (2)$$

where $R_i = \hat{I}_i^{depth} - I_i^{depth}$ and Δ_x and Δ_y are the spatial derivatives with respect to x-axis and y-axis. With this term, the overall loss function for depth becomes:

$$L_{depth} = \mathcal{L}_1^{Depth} + \mu \mathcal{L}_{grad} \quad (3)$$

where μ is a weighting coefficient set to 0.001.

2) *Deblurring loss*: Various loss functions have been proposed to train the DNNs for image deblurring. Pixel-wise content loss functions like L1 and L2 norm are the most common [43], [44].

To train 2HDED:NET, we test L1 norm and Charbonnier loss function [45], which is the smoothed version of L1. Charbonnier loss is calculated as a squared error between

the estimated deblurred image \hat{I}^{aif} and the ground truth AiF image I^{aif} :

$$\mathcal{L}_{charb} = \frac{1}{n} \sum_{i=1}^W \sum_{j=1}^H \sqrt{(\hat{I}_{i,j}^{aif} - I_{i,j}^{aif})^2 + \epsilon^2} \quad (4)$$

where ϵ is a hyper-parameter set to $1e-3$. This hyper-parameter acts as a pseudo-Huber loss and smooths the errors smaller than ϵ .

In a series of papers [23], [40], [46], the loss defined either as Charbonnier or L1 norm, is improved by requiring a high SSIM. This results into adding the supplementary term:

$$\mathcal{L}_{SSIM} = 1 - SSIM(\hat{I}_{i,j}^{aif}, I_{i,j}^{aif}) \quad (5)$$

which makes the complete loss function to be:

$$L_{deblur} = \mathcal{L}_{charb} + \Psi \mathcal{L}_{SSIM} \quad (6)$$

where Ψ is a weight set to 4.

3) *2HDED loss function*: With the depth and deblurring losses defined as in eq. 3 and 6, we define a total loss for 2HDED:NET training:

$$L_{2HDED} = L_{depth} + \lambda L_{deblur} \quad (7)$$

In our experiments, we use several versions of L_{2HDED} : with L_{depth} including or not \mathcal{L}_{smooth} , with L_{deblur} being either L1 norm or \mathcal{L}_{charb} , with or without SSIM loss. We noticed during the experiments that the model performance is very sensitive to this weighting value, which is why we paid close attention to the choice of λ . Starting from the idea that both tasks should be given the same importance, we evaluated the depth and deblurring losses separately during the training, and we settled λ such they have approximately the same contribution to the total loss. Then we fine tuned λ by performing a grid search and we found that $\lambda = 0.01$ is suitable for all versions of L_{HDED} .

E. Accuracy measures for DFD and image deblurring

To evaluate the accuracy of estimated depth map and deblurred images, we use common accuracy measures that have been widely reported in previous studies.

For the depth estimation, we compute the root mean square error (RMSE), relative error (Abs. Rel.), and thresholded accuracy δ as follows:

$$1) \text{ RMSE} = \sqrt{\frac{1}{n} \sum_{i=0}^n (\hat{I}_t^{depth} - I_t^{depth})^2}$$

$$2) \text{ Abs.Rel.} = \frac{1}{n} \sum_{i=0}^n \frac{|\hat{I}_t^{depth} - I_t^{depth}|}{I_t^{depth}}$$

$$3) \text{ Thresholded accuracy } (\delta) \text{ is the percentage of pixels such that: } \max\left(\frac{\hat{I}_t^{depth}}{I_t^{depth}}, \frac{I_t^{depth}}{\hat{I}_t^{depth}}\right) = \delta < \text{threshold}$$

To evaluate the deblurring, we resort to two well known metrics commonly used to measure the quality of images: Peak Signal to Noise Ratio (PSNR) and SSIM.

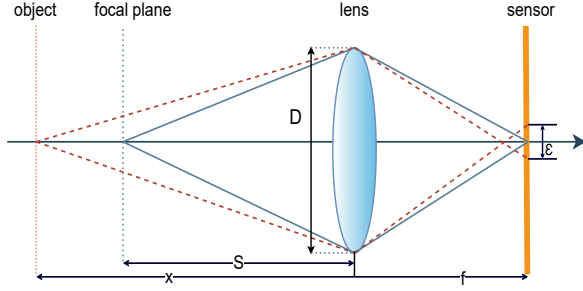


Fig. 3. The thin lens model: the COC diameter ε depends on the distance x of the object to the lens.

IV. DATASETS

2HDED:NET is trained with two types of ground truth, depth maps and AiF images. Since until recently, DFD and image deblurring have been considered separately, the existing solutions were developed around datasets dedicated either to one or the other application. The lack of datasets including defocused images, corresponding depth maps and AiF images, determined us to work on datasets for depth applications consisting in AiF images and depth ground truth, and to generate defocused images by blurring the AiF images. The synthetically defocused images have been used by many recent works [10], [11], [13] dedicated either to depth inference or image restoration.

Thus, our choice has been the NYU-Depth V2 dataset containing indoor scenes, and the Make3D dataset with outdoor scenes. The depth range of the datasets depends on the type of sensor used to capture the depth as well as the collection method. The depth range of NYU images is 0.7 to 10m and of Make3D 0 to 80m.

The NYU dataset comprises 230,000 pairs of RGB indoor images and their corresponding depth maps. In order to speed up the experiment, the training of 2HDED:NET has been run with a smaller dataset. We used the same split as [10], [11] i.e., 795 images for training and 654 for testing. The original size of the images captured by Microsoft Kinect is 640×480 pixels, but they were reduced to 561×427 pixels in our experiments.

The Make3D dataset consists of 534 RGB images and depth maps representing outdoor scenes. To train the 2HDED:NET under the same conditions as in [10], we split the dataset similarly, i.e., into 400 images for training and 134 images for testing.

To avoid overfitting, the training set has been increased by data augmentation. We adopted the data augmentation procedure addressed in [11]. Since we use defocus blur as a cue we do not apply any data augmentation process that can affect the blur information. In the first step all the images are centred scaled. For random flips, each individual sample is flipped horizontally by 50%.

A. Defocus Blur Simulation

To generate the realistic physical blur in the RGB images we adopt the procedure used by the authors in [47] to generate the SYNDOF dataset. To defocus an image, they start from

the thin lens model [48], commonly used in computer vision (Fig. 3). We used the same parameter values as [47] such as aperture size of 4.48 cm and focal length set to 0.07m. In Fig. 3, x is the distance to the object, f is the distance from the lens to the image sensor, D is the diameter of the aperture, S is the distance to the in-focus plane, and ε is the diameter of the circle of confusion (COC) calculated as:

$$\varepsilon = \alpha \frac{|x - S|}{x}, \text{ where } \alpha = \frac{f}{S} D \quad (8)$$

To generate blur in the AiF image, we apply Gaussian filters with a kernel with standard deviation $\rho = \varepsilon/4$. Similar to [47], ε is calculated based on the per pixel depth values. As a result we have defocus images with corresponding depth maps and AiF images.

V. RESULTS

For experimental results, we divided our analysis into the following sections:

- Depth estimation and image deblurring results with various loss functions. We tested simple solutions like L_{charb} for deblurring and L_1 for depth and we improved step by step our results by adding supplementary constraints consisting in SSIM for deblurring and smoothing for depth.
- Results with two heads and one head ablated to see the effectiveness of the two-head architecture.
- Finally, we compare our results to the state of the art results for depth or image deblurring, obtained on the NYU-v2 and Make3D benchmarks.

Our network is implemented in PyTorch. The entire training session takes approximately 9 hours on an NVIDIA Quadro GV100 GPU with 32 GB memory. We trained 2HDED:NET for 500 epochs with a batch size of 4 images. We use Stochastic Gradient Descent (SGD) optimizer with an initial learning rate of 0.0002. The initial learning rate is reduced 10-times after the first 300 epochs, this allows for large weight changes in the beginning of the learning process and small changes towards the end of the learning process. As for the total number of network parameters, our network is much lighter than [10]. The total number of parameters of 2HDED:NET is 41M, while [10] has 138M, which is three times higher than ours.

A. Effect of Loss Functions

In this subsection, we perform a set of experiments consisting in training the 2HDED:NET with the various loss functions described in section III-D. To select among the multiple options existing for our combined depth and deblur loss function, we adopt a simple to complex approach. In a first step, we use a photometric error for deblurring and L_1 norm for depth accuracy. For deblurring, we test with L_1 and Charbonnier loss functions, the latter being a smoothed version of L_1 . To ensure an equal contribution of the two components, the deblurring error is weighted by $\lambda = 0.01$. We maintain the principle of equal contribution over the entire experiment.

Table II presents results obtained on the NYU dataset. The depth estimation has a good accuracy even for this simple loss function. The RMSE is under 0.3 and there are not significant differences when the photometric error for deblurring switches from Charbonnier to L_1 , where the accuracy is only slightly worse. This is not the case for deblurring, where the use of Charbonnier improves the PSNR by $3dB$ comparing with L_1 , providing on average, a quality of $33.55dB$ for the test set. Therefore, we choose Charbonnier for the subsequent experiments.

In a second step, we alternately improve on deblur and depth losses by adding a SSIM based term to \mathcal{L}_{charb} and smoothing regularization to L_1 . These additional terms are weighted by $\Psi = 4$ and $\mu = 0.001$, respectively. The smoothing regularization improves the RMSE depth accuracy from 0.285 to 0.244 on average but it degrades by more than 1 dB the deblurring result. This apparently small difference in RMSE can impact significantly on the quality of depth maps as it can be seen from the example in Fig. 4, where new details are emerging when the smoothing regularization is added.

The introduction of SSIM term brings benefits to both depth estimation and deblurring. The RMSE decreases to 0.282 and the PSNR becomes higher by 0.3 dB on average. The deblurring results on simple L_1 loss and the default loss, which is $L_{charb} + \Psi(1 - SSIM)$, can be seen in Fig. 5.

Finally, we combine the photometric errors and the two regularizations – SSIM and smoothing – in a unique loss function. The network trained with this loss function achieves the best results both in depth accuracy and deblurring. The RMSE of depth touches the lowest level of 0.241 and the PSNR of the deblurred images is almost 35 dB. Some examples are depicted in Fig. 6 to 8 and commented in the next subsection.

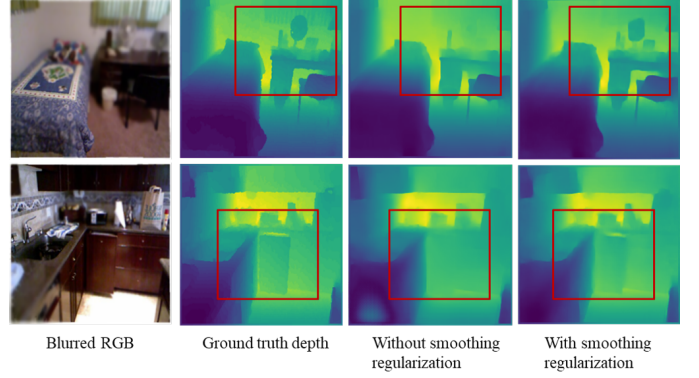


Fig. 4. Results with and without smoothing regularization for depth estimation on NYU-v2 dataset. The deblurring loss is \mathcal{L}_{charb} . The rectangular crops select areas where new details emerge when using smoothing regularization.

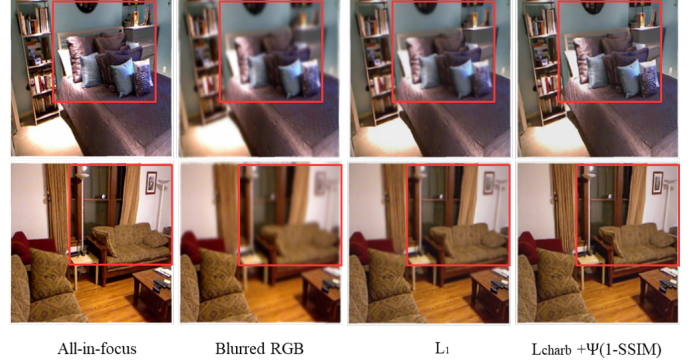


Fig. 5. Deblurring results with L_1 and $L_{charb} + \Psi(1 - SSIM)$ default loss on NYU-v2 dataset. The depth loss is L_1 .

TABLE II
RESULTS ON NYU-V2 DATASET WITH DIFFERENT LOSS FUNCTIONS FOR DEPTH ESTIMATION AND IMAGE DEBLURRING.

Loss Function	Depth Estimation					Image Deblurring	
	RMSE ↓	Abs. rel ↓	$\delta(1)$ ↑	$\delta(2)$ ↑	$\delta(3)$ ↑	PSNR ↑	SSIM ↑
$L_1^{Depth} + \lambda L_{charb}^{Deblur}$	0.285	0.035	0.820	0.880	0.970	33.55	0.983
$L_1^{Depth} + \lambda L_1^{Deblur}$	0.292	0.068	0.799	0.819	0.891	30.38	0.90
$(L_1^{Depth} + \mu L_{grad}) + \lambda L_{charb}^{Deblur}$	0.244	0.029	0.901	0.971	0.989	32.27	0.918
$L_1^{Depth} + \lambda(L_{charb}^{Deblur} + \Psi(1 - SSIM))$	0.282	0.031	0.833	0.895	0.901	33.85	0.981
$(L_1^{Depth} + \mu L_{grad}) + \lambda(L_{charb}^{Deblur} + \Psi(1 - SSIM))$	0.241	0.025	0.914	0.979	0.995	34.84	0.989

TABLE III
EFFECT OF ABLATING ONE HEAD. RESULTS ON NYU-V2 DATASET

Image Deblurring					
	$PSNR\uparrow$	$SSIM\uparrow$			
With both heads	34.849	0.989			
Without depth head	31.941	0.919			
Gain	2.899	0.07			
Depth Estimation					
	$RMSE\downarrow$	$Abs.\ rel\downarrow$	$\delta(1)\uparrow$	$\delta(2)\uparrow$	$\delta(3)\uparrow$
With both heads	0.24	0.025	0.91	0.97	0.99
Without deblurring head	0.29	0.075	0.84	0.89	0.94
Gain	0.05	0.05	0.07	0.08	0.05

B. Effect of head ablation

The 2HDED:NET is trained by using two kinds of ground truth values, the AiF image and the depth map. One is ingested by the deblurring head, the other one by the depth head. They contribute together to the training of the network as long as the loss function combines the depth and deblurring errors. Nevertheless, the network could be trained and still run by keeping a single head.

In this subsection, we evaluate the benefit of the two headed architecture to the overall accuracy of the model. Hence, we alternately remove one head and retrain the network by using either the AiF or depth error depending on what head is preserved. Table III shows the results. For image deblurring, when the depth head is ablated and the loss $\mathcal{L}_{charb} + \Psi(1 - SSIM)$ is used, the PSNR decreases by almost 3 dB, from 34.849 dB to 31.941 dB. Similarly, by ablating the deblurring head, the accuracy of the estimated depth maps becomes worse. On average, the RMSE increases by 0.05.

Thus, it is clear that 2HDED:NET achieves the best results when both heads are used together. Each head improves the results of the other one by complementing the ground truth, even if it is of a different nature.

C. Comparison with SoA methods for Depth Estimation and Image Deblurring

We compare 2HDED:NET with some state-of-the-art solutions based on neural networks for depth estimation and image deblurring. Since in the literature there are very few networks that solve simultaneously the problems of DFD and image deblurring [10], [30], we also consider recent methods dedicated exclusively to depth estimation. The blur is rarely taken into consideration in such cases [49]–[51], most of networks being trained on AiF images. Table IV presents in the left half, results for depth estimation obtained with networks trained on NYU and Make3D data set. For NYU dataset, the

best accuracy in terms of RMSE is obtained by Carvalho et al. [11] and Song et al. [13], both trained on defocused images with the sole purpose of generating depth maps. Their performances are very close, [13] outperforms [11] on *Abs.rel* but not on RMSE. The network in [13] gains by using instead of single image, couples of differently defocused images to estimate the depth, which means supplementary ground truth.

From the same category of networks using defocused images, there are [30] and [10]. They are the most representative for our comparison since these networks handle both depth maps and blurred images. On average, the depth maps accuracy of [10] is worse by 0.2 in RMSE comparing with the best result in [11]. Gur et al. [30] lags behind with a RMSE of 0.766 but the result is still remarkable given the fact that they use a self-supervised learning.

2HDED:NET is at half way between [11] and [10] with a RMSE of 0.241. In the category of networks handling both depth and deblurred images, our 2HDED:NET is the best in all metrics. We also present results for three recent networks trained on AiF images to generate exclusively depth maps. The average RMSE ranges between 0.433 and 0.579, well inferior to the results of [11] or [13] and to our result. This difference proves the effectiveness of the defocus in the training set. The defocus is an additional source of information, independent of the scene geometry, which is commonly exploited by neural networks.

Figure 6 depicts three examples of depth maps obtained with 2HDED:NET. The visual comparison with the ground truth shows high quality results. The smoothing regularization added to $L1$ loss instructs the network to produce depth maps with sharp edges and smooth, homogeneous regions that match well the ground truth and have significantly fewer artifacts. We evaluate the performance of 2HDED:NET also on Make3D dataset, which consists of outdoor scenes. The common approach to measure the depth accuracy on this data

TABLE IV
COMPARISON OF 2HDED:NET WITH SoA METHODS FOR DEPTH ESTIMATION AND IMAGE DEBLURRING ON NYU-V2 AND MAKE3D DATASETS.

			Depth Estimation						Deblurring	
NYU dataset										
Method	Depth	Deblur	RMSE ↓	Abs. rel ↓	$\delta(1) \uparrow$	$\delta(2) \uparrow$	$\delta(3) \uparrow$	PSNR ↑	SSIM ↑	
Tang et al. [49]	✓	×	0.579	0.132	0.826	0.936	0.992	–	–	
Chang et al. [50]	✓	×	0.433	0.087	0.930	0.990	0.999	–	–	
Dong et al. [51]	✓	×	0.537	0.146	0.799	0.951	0.988	–	–	
Song et al. [13]	✓	×	0.154	0.028	–	–	–	–	–	
Carvalho et al. [11]	✓	×	0.144	0.036	–	–	–	–	–	
Gur et al. [30]	✓	×	0.766	0.255	0.691	0.880	0.944	–	–	
Zhang et al. [35] (DnCNN)	×	✓	–	–	–	–	–	32.43	0.67	
Zhang et al. [36] (IrCNN)	×	✓	–	–	–	–	–	35.46	0.99	
Anwar et al. [10]	✓	✓	0.347	0.094	–	–	–	34.21	–	
2HDED:Net	✓	✓	0.244	0.029	0.914	0.979	0.995	34.85	0.99	
Make3D dataset										
	Depth	Deblur	C1-Error		C2-Error					
			RMSE ↓	Abs. rel ↓	RMSE ↓	Abs. rel ↓	PSNR ↑	SSIM ↑		
Fu et al. [12]	✓	×	3.970	0.157	7.32	0.162	–	–		
Gur et al. [30]	✓	×	8.822	0.568	10.147	0.575	–	–		
Zhang et al. [35] (DnCNN)	×	✓	–	–	–	–	23.16	0.68		
Zhang et al. [36] (IrCNN)	×	✓	–	–	–	–	27.09	0.70		
Anwar et al. [10]	✓	✓	2.560	0.213	0.079	0.202	21.07	–		
2HDED:Net	✓	✓	0.245	0.152	0.358	0.157	24.76	0.78		

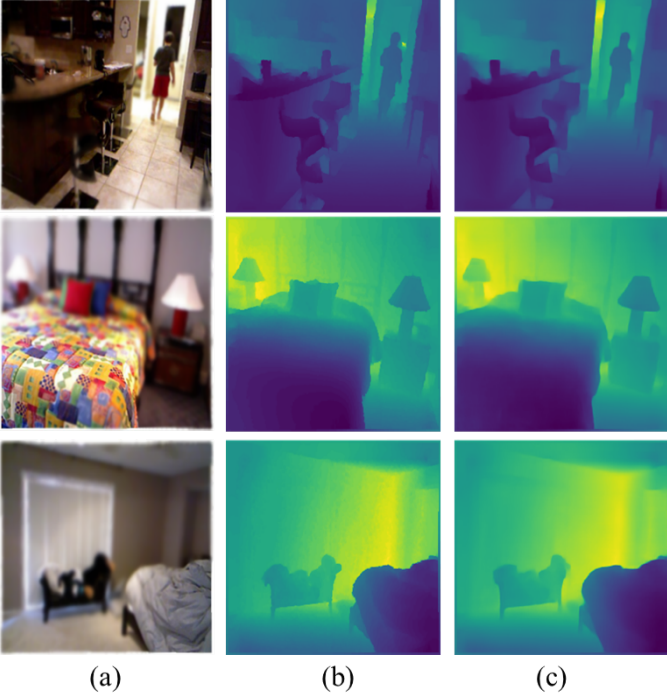


Fig. 6. 2HDED:NET results for depth estimation on NYU-v2 dataset using the default loss L_{2HDED} : (a) RGB defocused image (b) Depth ground truth (c) Estimated Depth.

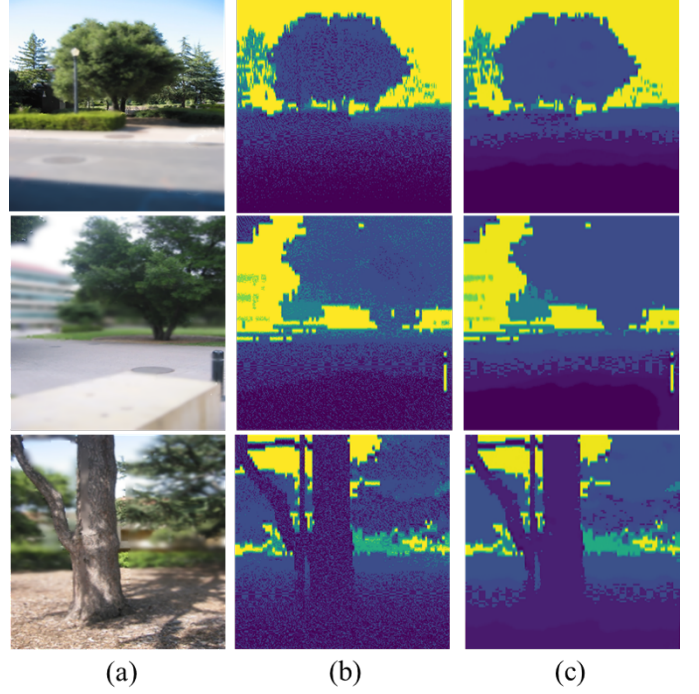


Fig. 7. 2HDED:NET results for depth estimation on Make3D dataset using the default loss L_{2HDED} : (a) RGB defocused image (b) Depth ground truth (c) Estimated depth.

set is to estimate errors on two depth ranges: C1 for depth up to 70m and C2 up to 80m [52]. The results for Make3D dataset are shown in the lower half of Table IV. Earlier methods [10], [12], [30], trained on Make3D dataset, are also displayed for comparison. As it can be seen, 2HDED:NET outperforms [12] and [30] in all metrics and for both ranges. As for [10], whose network like ours, estimates depth and AiF images, 2HDED:NET provides lower errors everywhere, except for C2 RMSE, where our result is inferior. Figure 7 depicts qualitative results for three different scenes. 2HDED:NET manages to correctly extract the depth of both near and distant regions.

In what concerns the deblurring, in order to have a fair comparison, we selected only methods that are tested on NYU and/or Make3D benchmarks. They are not numerous since these benchmarks are commonly used for depth inference not for deblurring. Thus, for the NYU dataset, we selected [10], [30], [53] as baseline and for Make3D dataset, only [10]. The results are shown in the right half of Table IV.

2HDED:NET performs better than the selected methods for NYU dataset, where it achieves an average PSNR of 34.85 dB. Comparing with [10], which is the main competitor, our results are superior by a margin of 0.64 dB. 2HDED:NET outperforms this method also on Make3D dataset, where the average PSNR is higher by 3db.

Some qualitative results are depicted in Fig. 8. On the first row, there are two scenes from the NYU dataset. For each scene, the AiF image 8(b), its artificially defocused counterpart 8(a) and the deblurred version output by 2HDED:NET 8(c) can be compared. It can be seen how the blur is reduced both from near and far ranges. Two small areas, one with the stickers on

the fridge in the foreground and the other with the margin of the hob closer to the camera are zoomed in on the second row. Fig. 8(c) shows how the details come to the surface after deblurring in both distant and near areas. 2HDED:NET works similarly on the second scene depicted in Fig. 8(d–f). A far and a near range patches are zoomed in order to prove the quality of the restored details.

For the outdoor scenes in the Make3D dataset, the quality of the restored image can be observed from the two examples in Fig. 8(g–l). The street light and the manhole cover that appear highly defocused in Fig. 8(g) are well restored in Fig. 8(i). Similarly, the tree branches in the second scene of Fig. 8(j) are obviously restored by 2HDED:NET in Fig. 8(l).

We also considered for comparison the two networks, IrCNN and DnCNN, proposed by Zhang Kai et al. in [35] and [36] for deblurring. Since the reported results were for other benchmarks, we retrained and tested the networks on our datasets. The DnCNN is under 2HDED:NET in PSNR and SSIM of the deblurred images, while IrDNN overcomes our solution by 0.6 dB on average on the NYU dataset, and by 2.33 dB on Make3D. Still, there are cases like the image in Fig. 10 with fine textures, where our network performs much better (a PSNR gain of 2 dB). It seems that fine textures are better restored by 2HDED:NET.

In evaluating 2HDED:NET, we paid a special attention to the comparison with the network of Anwar et al. [10], which like ours provides both depth maps and deblurred images but using a pipeline processing. In Fig. 9, we give an example of an image from the NYU dataset restored by both [10] and 2HDED:NET. Our method achieves a PSNR of 35.87 dB,



Fig. 8. 2HDED:NET results for deblurring on NYU-v2 and Make3D dataset. From left to right: (a) defocused image, (b) ground truth AiF image and (c) deblurred image. Similarly, (d), (e) and (f) for a different scene. Zoomed-in patches are shown below each scene.

which is almost 2 dB higher than that of [10] for the same image. The blur removal can be well observed on the areas delimited by the red rectangles: the light on the ceiling and the edges of the furniture. Another example, this time from the outdoor Make3D dataset, is depicted in Fig. 10. In this particular image, 2HDED:NET archives a PSNR of 37.19 dB, which is higher by almost 7 dB when compared to that obtained by [10]. The highly textured area of the wall, with tiles that are almost invisible in the image obtained by [10], is well restored in the image output by 2HDED:NET. Another advantage of 2HDED:NET by respect to [10] is the speed of computation. Once trained, 2HDED:NET generates very fast the restored image while in the case of [10], the restoration is a long process because of pixel-wise non-blind deconvolution.

VI. CONCLUSION AND FUTURE WORK

In this work, we presented a novel deep convolutional neural network that estimates depth and restores the AiF image from a single out-of-focus image. The proposed network has a two-headed architecture consisting in an encoder and two parallel decoders, each of which with its own role: one outputs the depth map and the other the deblurred image. The formulation of an architecture that estimates the depth maps while removing blur from out-of-focus images, distinguishes

our network from existing methods that are using pipeline processing. By parallelizing the tasks, the complexity of the network is reduced, while the depth estimation and blur removal work together toward performances that prove to be superior or close to the state-of-the-art results. Extensive tests on indoor and outdoor benchmarks have shown that 2HDED:NET outperforms the existing pipeline network in both DFD and image deblurring. For the novel architecture of 2HDED:NET, we have proposed a new loss function that fuses depth and AiF errors, traditionally used separately in deep learning.

Since we experimented with synthetically blurred datasets, our future work will focus on developing a real defocused dataset containing depth ground truth, AiF and naturally defocused images.

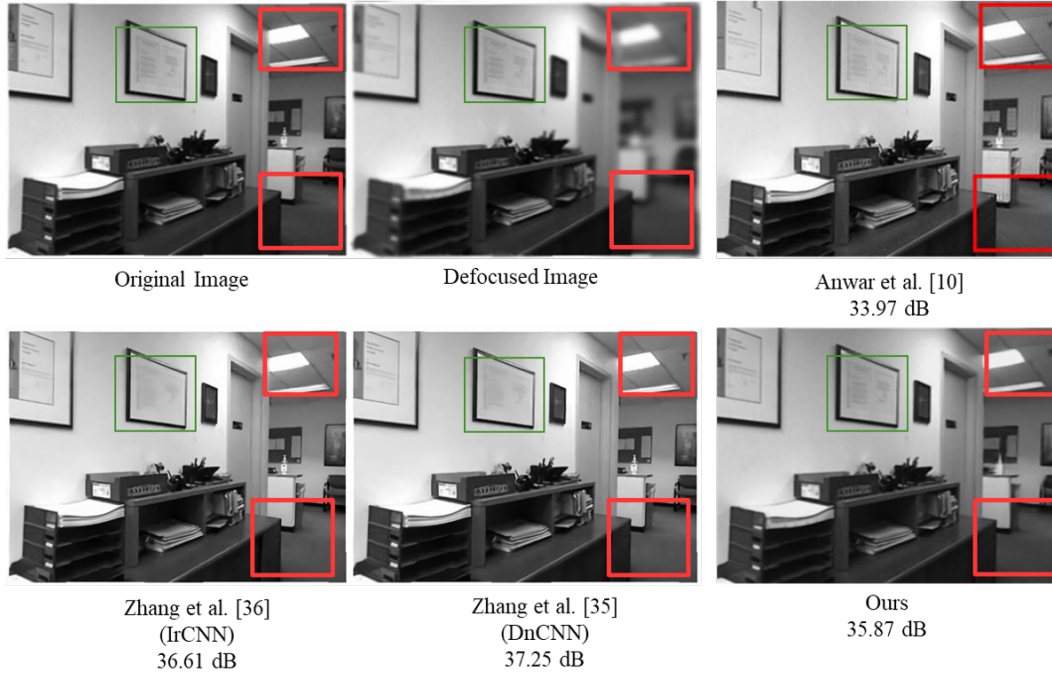


Fig. 9. Comparison of 2HDED:NET with the pipeline solution of Anwar et al. [10], and two general methods for image restoration [35], [36]: an example from NYU-v2 dataset.

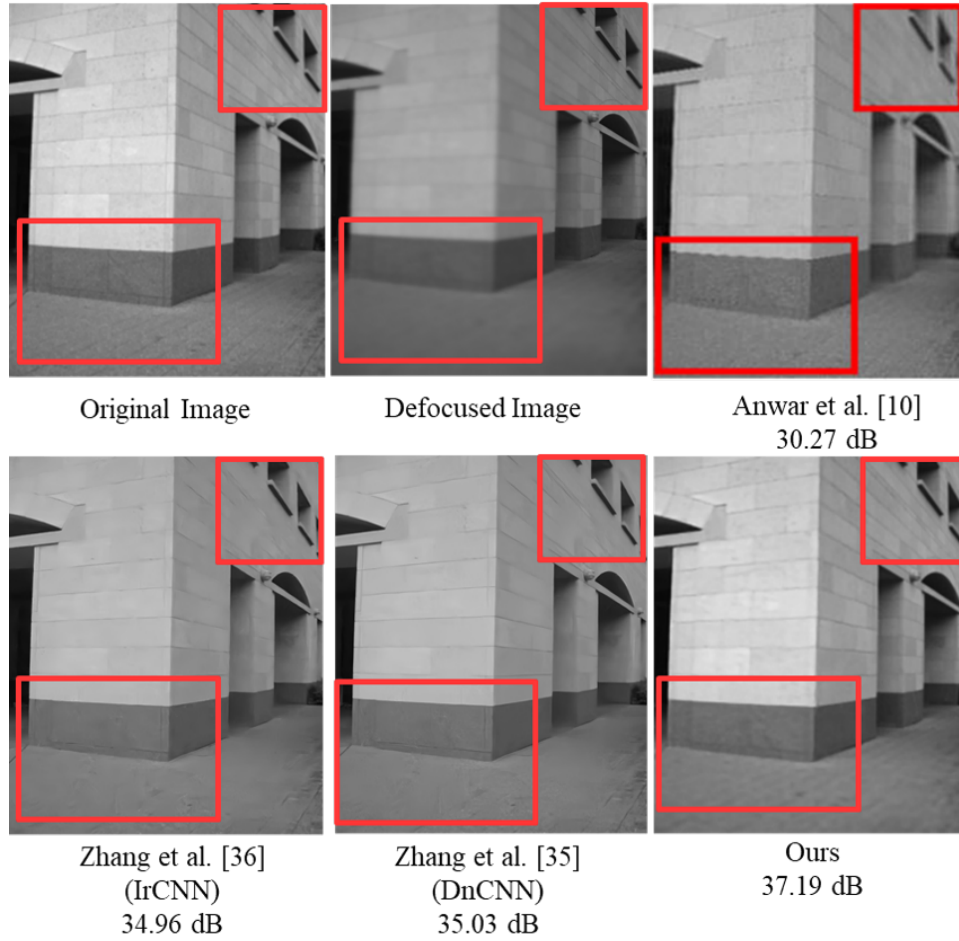


Fig. 10. Comparison of 2HDED:NET with the pipeline solution of Anwar et al. [10], and two general methods for image restoration [35], [36]: an example from Make3D dataset.

REFERENCES

- [1] C. Godard, O. Mac Aodha, and G. J. Brostow, "Unsupervised monocular depth estimation with left-right consistency," in *Proceedings of the IEEE conference on computer vision and pattern recognition*, 2017, pp. 270–279.
- [2] A. Saxena, M. Sun, and A. Y. Ng, "Make3d: Learning 3d scene structure from a single still image," *IEEE transactions on pattern analysis and machine intelligence*, vol. 31, no. 5, pp. 824–840, 2008.
- [3] D. Eigen, C. Puhrsch, and R. Fergus, "Depth map prediction from a single image using a multi-scale deep network," *Advances in neural information processing systems*, vol. 27, 2014.
- [4] C. Tang, C. Hou, and Z. Song, "Depth recovery and refinement from a single image using defocus cues," *Journal of Modern Optics*, vol. 62, no. 6, pp. 441–448, 2015.
- [5] A. Levin, R. Fergus, F. Durand, and W. T. Freeman, "Image and depth from a conventional camera with a coded aperture," *ACM transactions on graphics (TOG)*, vol. 26, no. 3, pp. 70–es, 2007.
- [6] M. Masoudifar and H. Pourreza, "Depth estimation and deblurring from a single image using an optimized-throughput coded aperture," *Journal of Electrical and Computer Engineering Innovations (JECEI)*, 2022.
- [7] C. Hazirbas, S. G. Soyer, M. C. Staab, L. Leal-Taixé, and D. Cremers, "Deep depth from focus," in *Asian Conference on Computer Vision*. Springer, 2018, pp. 525–541.
- [8] M.-B. Lien, C.-H. Liu, I. Y. Chun, S. Ravishankar, H. Nien, M. Zhou, J. A. Fessler, Z. Zhong, and T. B. Norris, "Ranging and light field imaging with transparent photodetectors," *Nature Photonics*, vol. 14, no. 3, pp. 143–148, 2020.
- [9] Z. Huang, J. A. Fessler, T. B. Norris, and I. Y. Chun, "Light-field reconstruction and depth estimation from focal stack images using convolutional neural networks," in *ICASSP 2020-2020 IEEE International Conference on Acoustics, Speech and Signal Processing (ICASSP)*. IEEE, 2020, pp. 8648–8652.
- [10] S. Anwar, Z. Hayder, and F. Porikli, "Deblur and deep depth from single defocus image," *Machine vision and applications*, vol. 32, no. 1, pp. 1–13, 2021.
- [11] M. Carvalho, B. Le Saux, P. Trouné-Peloux, A. Almansa, and F. Champagnat, "Deep depth from defocus: how can defocus blur improve 3d estimation using dense neural networks?" in *Proceedings of the European Conference on Computer Vision (ECCV) Workshops*, 2018, pp. 0–0.
- [12] H. Fu, M. Gong, C. Wang, K. Batmanghelich, and D. Tao, "Deep ordinal regression network for monocular depth estimation," in *Proceedings of the IEEE conference on computer vision and pattern recognition*, 2018, pp. 2002–2011.
- [13] G. Song and K. M. Lee, "Depth estimation network for dual defocused images with different depth-of-field," in *2018 25th IEEE International Conference on Image Processing (ICIP)*. IEEE, 2018, pp. 1563–1567.
- [14] L. Ruan, B. Chen, J. Li, and M.-L. Lam, "Aifnet: All-in-focus image restoration network using a light field-based dataset," *IEEE Transactions on Computational Imaging*, vol. 7, pp. 675–688, 2021.
- [15] A. Abuolaim and M. S. Brown, "Defocus deblurring using dual-pixel data," in *European Conference on Computer Vision*. Springer, 2020, pp. 111–126.
- [16] K. Zhang, W. Ren, W. Luo, W.-S. Lai, B. Stenger, M.-H. Yang, and H. Li, "Deep image deblurring: A survey," *arXiv preprint arXiv:2201.10700*, 2022.
- [17] C. Li, "A survey on image deblurring," *arXiv preprint arXiv:2202.07456*, 2022.
- [18] R. Caruana, "Multitask learning," *Machine learning*, vol. 28, no. 1, pp. 41–75, 1997.
- [19] S. Ruder, "An overview of multi-task learning in deep neural networks," *arXiv preprint arXiv:1706.05098*, 2017.
- [20] M. Crawshaw, "Multi-task learning with deep neural networks: A survey," *arXiv preprint arXiv:2009.09796*, 2020.
- [21] Y. Lu, M. Sarkis, and G. Lu, "Multi-task learning for single image depth estimation and segmentation based on unsupervised network," in *2020 IEEE International Conference on Robotics and Automation (ICRA)*. IEEE, 2020, pp. 10 788–10 794.
- [22] Y. Wang, Y.-H. Tsai, W.-C. Hung, W. Ding, S. Liu, and M.-H. Yang, "Semi-supervised multi-task learning for semantics and depth," in *Proceedings of the IEEE/CVF Winter Conference on Applications of Computer Vision*, 2022, pp. 2505–2514.
- [23] R. Xu, Z. Xiao, J. Huang, Y. Zhang, and Z. Xiong, "Edpn: Enhanced deep pyramid network for blurry image restoration," in *Proceedings of the IEEE/CVF Conference on Computer Vision and Pattern Recognition*, 2021, pp. 414–423.
- [24] K. Xian, J. Zhang, O. Wang, L. Mai, Z. Lin, and Z. Cao, "Structure-guided ranking loss for single image depth prediction," in *Proceedings of the IEEE/CVF Conference on Computer Vision and Pattern Recognition*, 2020, pp. 611–620.
- [25] S. Nazir, L. Vaquero, M. Mucientes, V. M. Brea, and D. Coltuc, "2HDED: Net for joint depth estimation and image deblurring from a single out-of-focus image," in *International Conference on Image Processing (ICIP)*, 2022, pp. 2006–2010.
- [26] I. Laina, C. Rupprecht, V. Belagiannis, F. Tombari, and N. Navab, "Deeper depth prediction with fully convolutional residual networks," in *2016 Fourth international conference on 3D vision (3DV)*. IEEE, 2016, pp. 239–248.
- [27] Y. Cao, Z. Wu, and C. Shen, "Estimating depth from monocular images as classification using deep fully convolutional residual networks," *IEEE Transactions on Circuits and Systems for Video Technology*, vol. 28, no. 11, pp. 3174–3182, 2017.
- [28] H. Jung, Y. Kim, D. Min, C. Oh, and K. Sohn, "Depth prediction from a single image with conditional adversarial networks," in *2017 IEEE International Conference on Image Processing (ICIP)*. IEEE, 2017, pp. 1717–1721.
- [29] M. Carvalho, B. Le Saux, P. Trouné-Peloux, A. Almansa, and F. Champagnat, "On regression losses for deep depth estimation," in *2018 25th IEEE International Conference on Image Processing (ICIP)*. IEEE, 2018, pp. 2915–2919.
- [30] S. Gur and L. Wolf, "Single image depth estimation trained via depth from defocus cues," in *Proceedings of the IEEE/CVF Conference on Computer Vision and Pattern Recognition*, 2019, pp. 7683–7692.
- [31] S. Nah, T. Hyun Kim, and K. Mu Lee, "Deep multi-scale convolutional neural network for dynamic scene deblurring," in *Proceedings of the IEEE conference on computer vision and pattern recognition*, 2017, pp. 3883–3891.
- [32] X. Tao, H. Gao, X. Shen, J. Wang, and J. Jia, "Scale-recurrent network for deep image deblurring," in *Proceedings of the IEEE conference on computer vision and pattern recognition*, 2018, pp. 8174–8182.
- [33] O. Kupyn, V. Budzan, M. Mykhailych, D. Mishkin, and J. Matas, "Deblurgan: Blind motion deblurring using conditional adversarial networks," in *Proceedings of the IEEE conference on computer vision and pattern recognition*, 2018, pp. 8183–8192.
- [34] J. Lee, H. Son, J. Rim, S. Cho, and S. Lee, "Iterative filter adaptive network for single image defocus deblurring," in *Proceedings of the IEEE/CVF Conference on Computer Vision and Pattern Recognition*, 2021, pp. 2034–2042.
- [35] K. Zhang, W. Zuo, Y. Chen, D. Meng, and L. Zhang, "Beyond a gaussian denoiser: Residual learning of deep cnn for image denoising," *IEEE transactions on image processing*, vol. 26, no. 7, pp. 3142–3155, 2017.
- [36] K. Zhang, W. Zuo, S. Gu, and L. Zhang, "Learning deep cnn denoiser prior for image restoration," in *Proceedings of the IEEE conference on computer vision and pattern recognition*, 2017, pp. 3929–3938.
- [37] Z. Zha, B. Wen, X. Yuan, J. T. Zhou, J. Zhou, and C. Zhu, "Triply complementary priors for image restoration," *IEEE Transactions on Image Processing*, vol. 30, pp. 5819–5834, 2021.
- [38] Z. Zha, X. Yuan, J. Zhou, C. Zhu, and B. Wen, "Image restoration via simultaneous nonlocal self-similarity priors," *IEEE Transactions on Image Processing*, vol. 29, pp. 8561–8576, 2020.
- [39] G. Huang, Z. Liu, L. Van Der Maaten, and K. Q. Weinberger, "Densely connected convolutional networks," in *Proceedings of the IEEE conference on computer vision and pattern recognition*, 2017, pp. 4700–4708.
- [40] X. Zhang, F. Wang, H. Dong, and Y. Guo, "A deep encoder-decoder networks for joint deblurring and super-resolution," in *2018 IEEE International Conference on Acoustics, Speech and Signal Processing (ICASSP)*. IEEE, 2018, pp. 1448–1452.
- [41] J. Hu, M. Ozay, Y. Zhang, and T. Okatani, "Revisiting single image depth estimation: Toward higher resolution maps with accurate object boundaries," in *2019 IEEE Winter Conference on Applications of Computer Vision (WACV)*. IEEE, 2019, pp. 1043–1051.
- [42] C. Godard, O. Mac Aodha, M. Firman, and G. J. Brostow, "Digging into self-supervised monocular depth estimation," in *Proceedings of the IEEE/CVF International Conference on Computer Vision*, 2019, pp. 3828–3838.
- [43] R. Timofte, R. Rothe, and L. Van Gool, "Seven ways to improve example-based single image super resolution," in *Proceedings of the IEEE conference on computer vision and pattern recognition*, 2016, pp. 1865–1873.
- [44] B. Lim, S. Son, H. Kim, S. Nah, and K. Mu Lee, "Enhanced deep residual networks for single image super-resolution," in *Proceedings of the IEEE conference on computer vision and pattern recognition workshops*, 2017, pp. 136–144.

- [45] P. Charbonnier, L. Blanc-Feraud, G. Aubert, and M. Barlaud, "Two deterministic half-quadratic regularization algorithms for computed imaging," in *Proceedings of 1st International Conference on Image Processing*, vol. 2. IEEE, 1994, pp. 168–172.
- [46] A. Abuolaim, R. Timofte, and M. S. Brown, "Ntire 2021 challenge for defocus deblurring using dual-pixel images: Methods and results," in *Proceedings of the IEEE/CVF Conference on Computer Vision and Pattern Recognition*, 2021, pp. 578–587.
- [47] J. Lee, S. Lee, S. Cho, and S. Lee, "Deep defocus map estimation using domain adaptation," in *Proceedings of the IEEE/CVF Conference on Computer Vision and Pattern Recognition*, 2019, pp. 12 222–12 230.
- [48] M. Potmesil and I. Chakravarty, "A lens and aperture camera model for synthetic image generation," *ACM SIGGRAPH Computer Graphics*, vol. 15, no. 3, pp. 297–305, 1981.
- [49] M. Tang, S. Chen, R. Dong, and J. Kan, "Encoder-decoder structure with the feature pyramid for depth estimation from a single image," *IEEE Access*, vol. 9, pp. 22 640–22 650, 2021.
- [50] J. Chang and G. Wetzstein, "Deep optics for monocular depth estimation and 3d object detection," in *Proceedings of the IEEE/CVF International Conference on Computer Vision*, 2019, pp. 10 193–10 202.
- [51] X. Dong, M. A. Garratt, S. G. Anavatti, and H. A. Abbass, "Mobilexnet: An efficient convolutional neural network for monocular depth estimation," *arXiv preprint arXiv:2111.12334*, 2021.
- [52] M. Liu, M. Salzmann, and X. He, "Discrete-continuous depth estimation from a single image," in *Proceedings of the IEEE Conference on Computer Vision and Pattern Recognition*, 2014, pp. 716–723.
- [53] J. Qiu, X. Wang, S. J. Maybank, and D. Tao, "World from blur," in *Proceedings of the IEEE/CVF Conference on Computer Vision and Pattern Recognition*, 2019, pp. 8493–8504.



Manuel Mucientes is an Associate Professor at the CiTIUS of the University of Santiago de Compostela, Spain. His main research interest is artificial intelligence applied to the following areas: computer vision for object detection and tracking; machine learning; process mining. He has authored more than 100 scientific papers in these fields of research.



Daniela COLȚUC received MSc, PhD degrees and habilitation in Electronics, Telecommunications and Information Technology from Univ. POLITEHNICA of Bucharest, Romania. She is currently full professor with this university. She has served also as invited professor at Univ. Jean Monet in St. Etienne and Univ. de Lyon, France. She has a sound background in Information theory with applications in image processing. In the recent years, she has worked in computational imaging.

VII. BIOGRAPHY SECTION



Saqib Nazir is a Ph.D. student at CEOSpace Tech. of Polytechnic University of Bucharest (UPB), Romania. He received his Masters and Bachelors's degree in Computer Science from COMSATS University Islamabad, Pakistan. His role as an Early Stage Researcher in the MENELOAS-NT Project is to acquire depth from defocus images using state of the art deep learning methods. His areas of interest include 'Computer Vision, Image analysis, Machine & Deep Learning'.



Lorenzo Vaquero is a Ph.D. student at the CiTIUS of the University of Santiago de Compostela, Spain. He received the B.S. degree in Computer Science in 2018 and the M.S. degree in Big Data in 2019. His research interests are visual object tracking and deep learning for autonomous vehicles.



Víctor M. Brea is an Associate Professor at CiTIUS, University of Santiago de Compostela, Spain. His main research interest lies in Computer Vision, both on deep learning algorithms, and on the design of efficient architectures and CMOS solutions. He has authored more than 100 scientific papers in these fields of research.